Korean J. Chem. Eng., **31**(1), 62-67 (2014)
DOI: 10.1007/s11814-013-0180-y

pISSN: 0256-1115
eISSN: 1975-7220

Fabrication and characterization of silicon nanostructures based on metal-assisted chemical etching

Wendong Zhang*,, Xuge Fan*,**, Shengbo Sang*,**, Pengwei Li*,**, Gang Li*,**, Yongjiao Sun*,**, and Jie Hu*,**,†**

*MicroNano System Research Center, Information Engineering College, Taiyuan University of Technology, Taiyuan, Shanxi, China
**Key Lab of Advanced Transducers and Intelligent Control System, Ministry of Education, Taiyuan University of Technology, Taiyuan, Shanxi, China
(*Received 27 May 2013 • accepted 16 September 2013*)

Abstract−We present a facile method to fabricate one-dimensional Si nanostructures based on Ag-induced selective etching of silicon wafers. To obtain evenly distributed Si nanowires (SiNWs), the fabrication parameters have been optimized. As a result, a maximum of average growth rate of 0.15 μm/min could be reached. Then, the fabricated samples were characterized by water contact angle (CA) experiments. As expected, the as-etched silicon samples exhibited a contact angle in the range of 132°-136.5°, whereas a higher contact angle (145°) could be obtained by chemical modification of the SiNWs with octadecyltrichlorosilane (OTS). Additionally, Raman spectra experiments have been carried out on as-prepared nanostructures, showing a typical decreasing from 520.9 cm^{-1} to 512.4 cm^{-1} and an asymmetric broadening, which might be associated with the phonon quantum confinement effect of Si nanostructures.

Keywords: Metal-assisted Chemical Etching, Si Nanostructures, Si Nanowires, Wettability, Raman Spectra

INTRODUCTION

One-dimensional nanostructures, including nanowires, nanotubes, nanorods and nanopores, have attracted increasing attention because of their size effects and novel physical characteristics [1,2]. Among many others, silicon nanowires are of particular interest since they can be widely used as a building blocks for devices in nanoelectronics [3], opto-electronics [4], energy conversion [5-7], energy storage [8,9] and biochemical sensors [10,11], due to their compatibility with the existing Si technology, and their known structural, electronic, and optical properties. To prepare Si nanostructures, various kinds of methods have been developed, such as chemical vapor deposition [12], molecular beam epitaxy [13], laser ablation [14], template assisted growth [15], thermal evaporation [16], oxide-assisted growth [17], supercritical-fluid-based and solution-based growth [18], and lithography-related etching methods [19-21]. However, most of these methods require complicated equipment with difficult work conditions such as high temperature, high vacuum, long processing time or hazardous silicon precursors, which make them time consuming and expensive.

Recently, a facile low-temperature method has been developed based on a metal-assisted chemical etching (MaCE) that can overcome the above-mentioned limitations. Using this method, the large area growth of vertically aligned crystalline silicon nanowires can be readily fabricated on Si substrates via a redox reaction between silicon and silver ions in an aqueous solution containing silver nitrate ($AgNO_3$) and hydrofluoric acid (HF) [22-25]. In addition, highly oriented SiNWs array and Si nanostructures can also be prepared by MaCE of Si wafers in HF-based aqueous solution containing oxidizing agents, such as $Fe(NO_3)_3$ or H_2O_2 [26-29]. In the metal-assisted chemical etching of Si, only noble metals (Pt, Au, Ag, Pd) can be practically used to assist the etching of Si [22,26,27]. It has been well-accepted that the chemical reactions occur preferentially near the noble metal. Because of its inherent simplicity, low cost, easy process control, and reproducibility, MaCE is likely to be used even more extensively as a reliable method for fabricating Si nanostructures [28].

In this paper, we present a method to fabricate Si nanostructures including Si nanoporous and SiNWs array in the HF/$AgNO_3$ solution using MaCE method. By optimizing the reaction conditions such as solution concentration, etching time and reaction temperature, bundle SiNWs array and nanoporous could be obtained. The etching mechanism of Si nanostructures has also been investigated. Furthermore, water contact angle experiments have been carried out on silicon nanostructures and OTS coated SiNWs. Finally, Raman spectra of Si nanostructures fabricated via MaCE method were also analyzed.

EXPERIMENTAL SECTION

In our experiment, commercially available p-type Si (100) wafers with a resistivity of 0.014-0.015 Ω·cm were used as substrates for the preparation of silicon nanostructures. $AgNO_3$ (>99.8%), hydrofluoric acid (>40%), sulfuric acid (95-98%), nitric acid (65-68%), hydrogen peroxide 30% and hydrochloric acid 37% were purchased from Tianjin Kermel Chemical Reagent Co., Ltd. Ethanol, toluene and acetone were purchased from Sinopharm Chemical Reagent Co., Ltd. Octadecyltrichlorosilane (OTS) was purchased from Sigma-Aldrich.

Prior to the formation of Si nanostructures, the polished Si wafer

†To whom correspondence should be addressed.
E-mail: hujie@tyut.edu.cn

was cut into rectangular shape with dimension of 1 cm×1 cm and sufficiently cleaned in a mixture of H_2SO_4 and H_2O_2 solution with a volume ratio of 3 : 1 for 10 min to remove organic materials. Afterward, the samples were washed in acetone and ethanol each for 5 min, using an ultrasonic cleaner. Then, the Si pieces were rinsed with deionized (DI) water, followed by dipping in 5% HF solution to remove any oxides. Finally, to fabricate Si nanostructures by electroless etching, the cleaned wafers were transferred into an Ag deposition solution containing 5 M HF and 0.02 M $AgNO_3$ for 10 min at room temperature. Then the Ag deposited samples were immersed in a certain concentration of etching solution, while the etching temperature and time were varied. The etched samples were rinsed with concentrated HNO_3 solution to remove thick Ag layer. At last, the samples were washed with DI water for several times, and blown dry with nitrogen for further investigations.

The morphologies of fabricated Si nanostructures were characterized by scanning electron microscopy (SEM, JSM-6700). A homemade water contact angle measurement system was introduced to measure the wettability of polished Si wafer and nanostructures. The DI water droplet is about 2.5 μL and each measurement was repeated three times. To lower the surface energy, the fabricated Si nanostructures were immersed in a 1 mmol/L OTS-toluene solution for 60 min, then the OTS coated nanostructures were washed by toluene. The Raman spectroscopy measurement was carried out using Raman Microscope (In Via), and it was performed with an Ar^+ laser operating at 514.5 nm with 6 mW power, a 3,000 *l*/mm grating and a 50× objective lens, at constant temperature (293 K) and constant humidity (40%) in a clean room.

RESULTS AND DISCUSSION

Fig. 1(a) shows a typical SEM image of the as-prepared sample, and clearly the surfaces of etched Si samples are covered with dendrites nanostructures, which is in accordance with relevant previous literatures [22-25], demonstrating the tree-like nanostructures were silver. It can be explained that Ag nanoparticles gradually grew into Ag nanoclusters and consequently agglomerated to develop the Ag dendritic structures rather than a compact Ag film, which results into selective oxidation and dissolution of Si in the aqueous HF/$AgNO_3$ solution.

Fig. 1(b)-(d) show SEM images of Si samples etched in 0.02 mol/L $AgNO_3$ and 10% HF solution under 50 °C for different times, and all of the etched Si samples have been treated by the concentrated HNO_3. When the Si sample was etched for 10 min, the nanoporous were formed on the surface (as Fig. 1(b)). With the increasing of the etching time, the nanostructures gradually evolved into SiNWs array (as Fig. 1(c)). When the etching time was up to 120 min, most of SiNWs collapsed or disappeared due to over-etching (as Fig. 1(d)). Therefore, in the following experiments, the etching time was mainly set as 60 min.

A similar bundle SiNWs array can still be prepared with higher density and more uniform distribution, when etching temperature

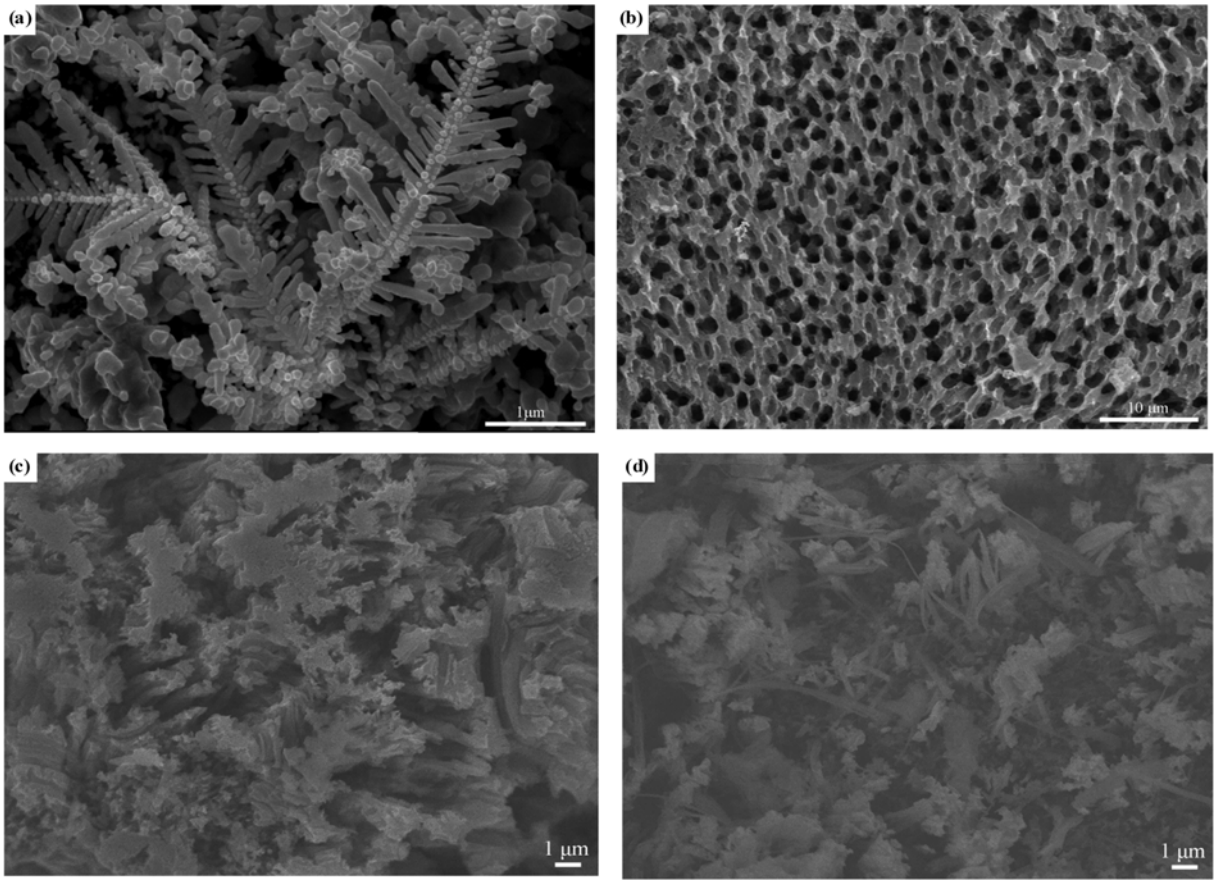

Fig. 1. SEM images of silver dendrite film wrapping in the Si samples (a) and Si nanostructure etched with 0.02 mol/L $AgNO_3$ and 10% HF at 50 °C for 10 min (b), 60 min (c), and 120 min (d).

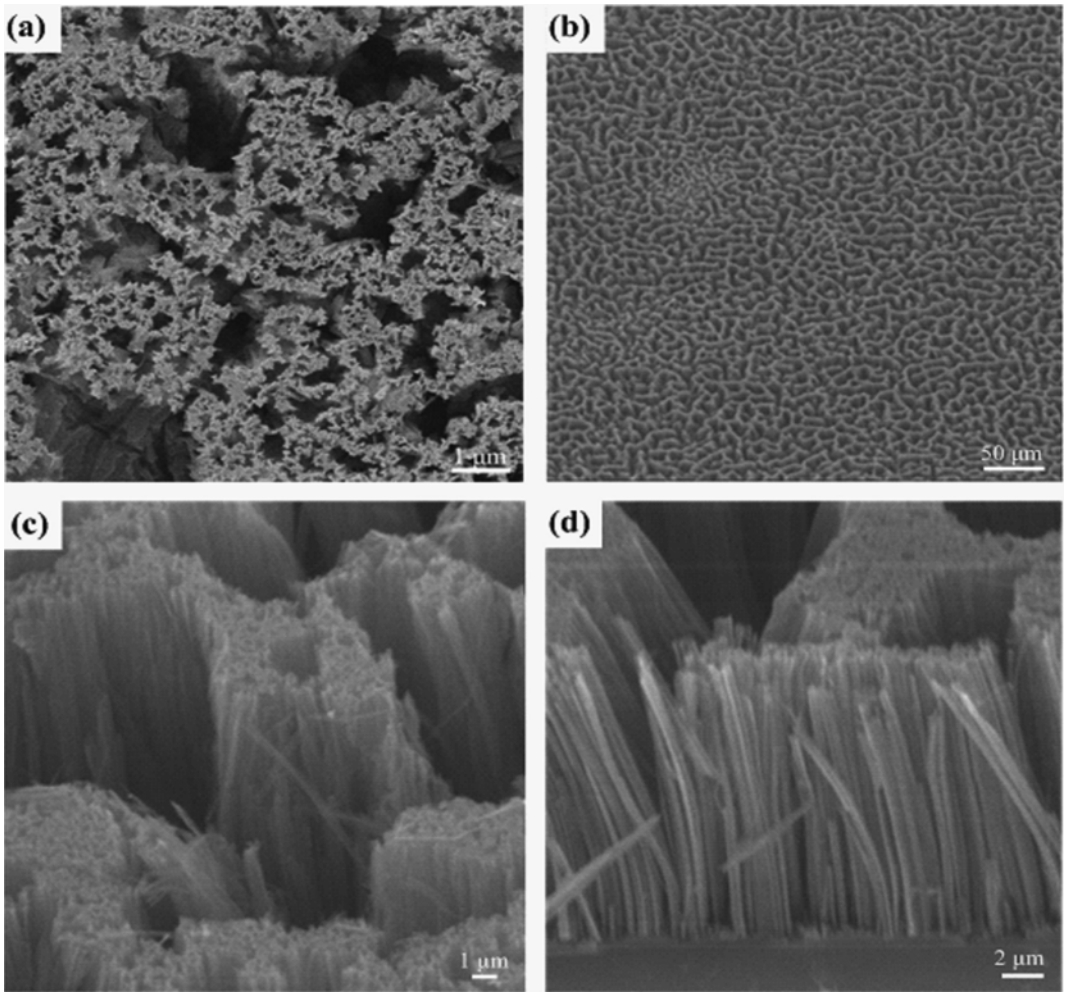

Fig. 2. (a) Top-view SEM image of silicon nanowires prepared with 0.02 mol/L $AgNO_3$ and 10% HF at 20 °C for 60 min. (b) Similar results obtained with 0.03 mol/L $AgNO_3$ and 10% HF at 50 °C for 60 min. (c) high magnification image and (d) tilted-view image of (b).

is decreased from 50 °C to 20 °C. Fig. 2(a) shows the SEM image of Si samples etched in the solution of 0.02 mol/L $AgNO_3$ and 10% HF under 20 °C for 60 min. The bundle SiNWs structures were closely interconnected and arranged perpendicular to the Si (100) surface. Fig. 2(b-c) show different magnification images of Si nanostructures prepared in 0.03 mol/L $AgNO_3$ and 10% HF at 50 °C for 60 min. Fig. 2(d) shows the cross-sectional image of SiNWs array with the length of nearly 15 μm. According to these results, evenly distributed and ordered SiNWs array can be prepared under this condition.

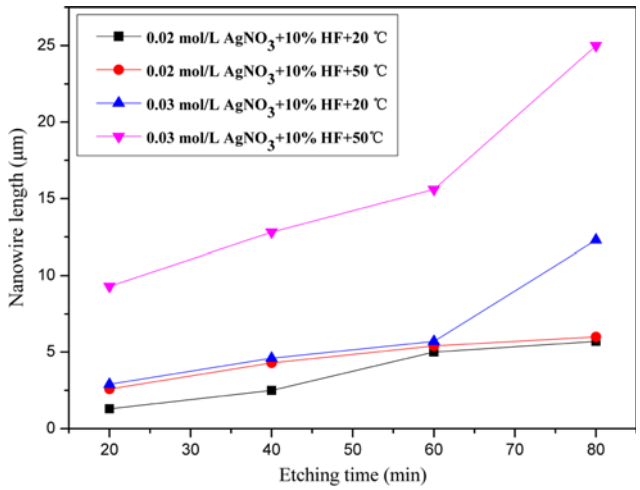

Fig. 3. Si nanowires length versus etching time, obtained with samples prepared under different reaction conditions.

Time-dependent etchings of Si samples were performed to discuss the growth rate of SiNWs. Fig. 3 exhibits the relationship between the length of the fabricated SiNWs and etching time under different conditions where the length of the SiNWs increased proportionally with increasing etching time up to 60 min. The maximum length of nanowires is nearly 15 μm and the maximum of average growth rate is about 0.15 μm/min. Specifically, the SiNWs array grew fastest in solution of 0.03 mol/L $AgNO_3$ and 10% HF at 50 °C, which is increased from 9.3 μm to 15 μm. While in the solution of 0.02 mol/L $AgNO_3$ and 10% HF at 20 °C, the SiNWs array grew lowest, which is only increased from 1.3 μm to 5 μm. It illustrated that both concentration and temperature could influence the growth rates, and the concentration is the primary influencing factor.

In the whole reaction process of MaCE in the HF/$AgNO_3$ solution, Ag nanoparticles are playing an important role of catalyst in elec-

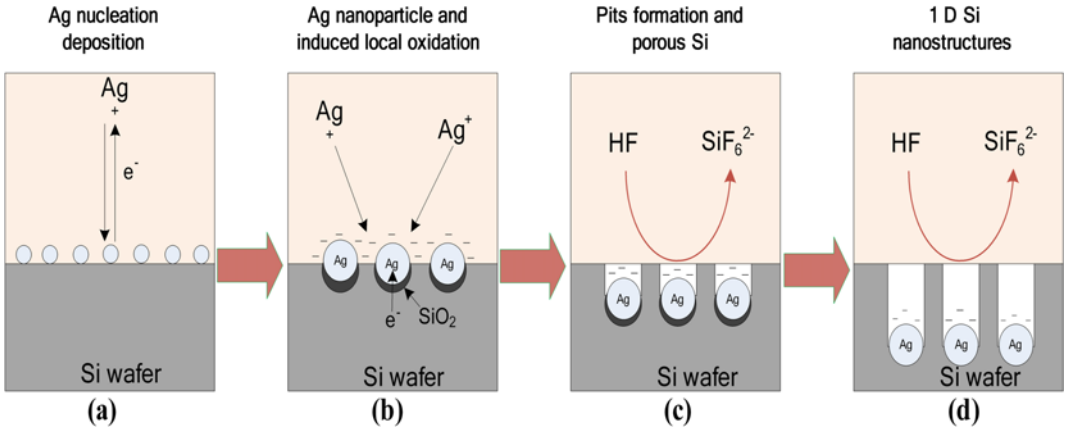

Fig. 4. Scheme of a growth mechanism for the SiNWs etched in the $AgNO_3$/HF solution. (a) Ag nucleation deposition. (b) Ag nanoparticle and induced local oxidation. (c) Pits formation. (d) Final Si nanostructures.

trochemical etching of Si in HF solution where deep cylindrical nano pores were formed in [100] silicon [30-33]. The mechanism of formation of the vertically aligned SiNWs array can be explained as being a self-assembled Ag-induced selective etching process based on localized microscopic electrochemical cell model, which is presented in Fig. 4. The process depends on the continuous galvanic displacement of Si by Ag ions being reduced to Ag, which forms many local nano-electrochemical cells on the Si surface. The original Ag nanoparticles serve as active cathode, and the Si area surrounding the Ag nanoparticles serve as active anode. Fig. 4(a) shows the process of Ag nucleation deposition. Ag ions adjacent to the Si wafer attract intensively electrons from the valence band of Si with a product of Ag atoms. Then Ag atoms simultaneously congregate into Ag nuclei and deposit uniformly on the Si substrate to form nanoclusters. After that, Si wafer beneath the Ag nanoparticles was oxidized to SiO_2 and the oxidized surface was etched away by HF (as Fig. 4(b)). The reaction product SiF_6^{2-} was dissolved into the solution. According to the above reaction process, those locations where Ag nuclei existed continuously presented oxidation and reduction reaction. With the increase of reaction time, the pits were produced at the same positions, which made Ag nanoclusters sink into such pits. The size of pits on Si surface increases initially as dimensions of Ag nanoclusters increase and gradually leads to the production of porous structures (as Fig. 4(c)). Once the Ag nanoclusters get trapped into the Si pores, they sink deeper and deeper, which causes the positions around Ag nanoparticles to form SiNWs or nanoporous (as Fig. 4(d)).

To investigate wettability, water contact angle measurements were made to test polished Si substrate and as-prepared nanostructures. Fig. 5(a) shows the optical image of contact angle of a DI water droplet on the surface of polished Si substrate. It can be seen that the CA is 72° and indicated that the polished Si wafer is hydrophilic. Fig. 5(b) presents the CA for bundle SiNWs array sample, which was prepared with 0.02 mol/L $AgNO_3$ and 10% HF etching solution at 50 °C for 60 min, and it is about 133°. For the other fabricated SiNWs samples, their CAs is in the range of 132°-136.5°. In addition, we performed chemical surface modification of SiNWs array by the self-assembled OTS monolayer. The OTS coated sample has the highest contact angle, which is about 145°, as shown in Fig. 5(c). Compared with uncoated sample, the CA of the OTS coated SiNWs further increased by 12°, which could be explained that the surface energy of the SiNWs was reduced. It demonstrated that the OTS coated SiNWs almost has a superhydrophobic surface. The observed hydrophobic characteristics for bundle SiNWs array could be explained by Cassie's model [34]. When a water droplet is placed on the surface of Si nanostructures, it is possible that the bundled SiNW structures might have the functionality of delaying the diffusion of air below the water droplet, which produces a phenomenon that abundant air could be trapped in the interval of the nanowire structures. Based on Cassie's model, a greater amount of air staying in the Si nanostructures would enhance the hydrophobicity of the Si sample surfaces [35,36].

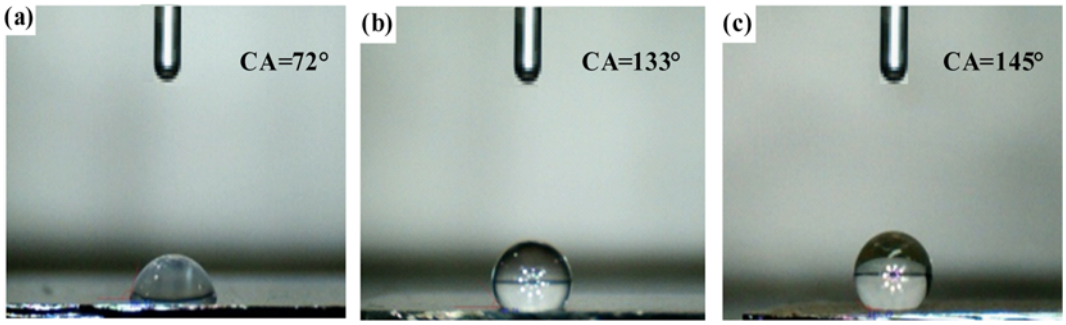

Fig. 5. Photographs showing different CAs on the surface of different samples. (a) Polished Si substrate. (b) Bundle SiNWs. (c) Bundle SiNWs after surface treatment by self-assembled OTS monolayer.

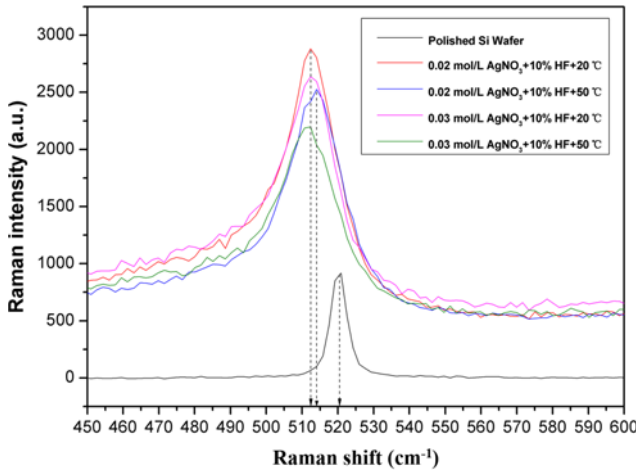

Fig. 6. The comparative Raman spectra of polished Si wafer and nanostructures after being etched in the solution of $AgNO_3$ and HF under different reaction conditions.

Finally, micro-Raman with excitation wavelengths of 514.5 nm was used to characterize the as-prepared nanostructures to address their lattice vibrational properties. Fig. 6 shows a comparison of Raman spectra of Si samples etched under four conditions and polished Si wafer. A Raman peak at 520.9 cm^{-1} was measured for the polished Si wafer, which can be explained by the scattering of the first-order optical phonon for crystalline Si [37]. The Raman spectra of Si nanostructures generally show a peak at 512.4 cm^{-1} and 514 cm^{-1}. It can be concluded from the Raman spectra that the first-order Raman peaks of etched Si nanostructures have an obvious red shift (the maximum shift value reaches nearly 9 cm^{-1}) and exhibits an asymmetric broadening toward the low-energy side. This asymmetric broadening and obvious downshift might be associated with the phonon quantum confinement effect of SiNWs [38]. Besides, they are mainly due to laser-induced inhomogeneous heating since the bundle SiNWs is freestanding on the substrate and a poor thermal anchorage to the substrate is anticipated [39,40].

CONCLUSIONS

We have demonstrated a relatively simple, cheap, and rapid method for the fabrication of Si nanostructures using p-type (100) Si substrates and a MaCE based technique with aqueous HF/$AgNO_3$ etching solution. The vertically aligned silicon nanowires have been prepared by optimization the etching parameters, including etching time, etching solution concentration and temperature. The results show a maximum nanowire length of 15 μm obtained with an average etch rate of about 0.15 μm/min. The formation of SiNWs could be attributed to the selective etching of Si substrate directly deposition with Ag nanoclusters via self-assembled nano-electrochemical process. SiNWs array takes place where there are no Ag nanoparticles depositions. The water contact angle experiments showed that the surface of etched Si nanostructures was hydrophobic and, as expected, their hydrophobicity could be significantly enhanced by surface coated of OTS. Finally, Raman spectra of the fabricated silicon nanostructures showed a clear redshift and an asymmetric broadening compared to that of the flat silicon wafer, which might be related to the phonon quantum confinement effect of Si nanostructures and laser-induced inhomogeneous heating. We believe that the method presented in this work is simple and low cost, which might not only be useful for optoelectronics and nano-electronics but also have potential applications in the fields of solar cells and biology.

ACKOWLEDGEMENTS

This research was supported by a grant from the National Natural Science Foundation of China (no. 51205274, no. 51205273), the Shanxi Province Science Foundation for Youths (no. 2013021017-2), the Shanxi Scholarship Council of China (no. 2013-035), China Postdoctoral Science Foundation (no. 2013M530894), and Excellent Innovation Programs for Postgraduate in Shanxi Province (no. 20110348).

REFERENCES

1. C. N. R. Rao, F. L. Deepak, G. Gundiah and A. Govindraj, *Prog, Solid State Chem*., **31**(1-2), 5 (2003).
2. Y. Xia, P. Yang, Y. Sun, Y. Wu, B. Mayers, B. Gates, Y. Yin, F. Kim and H. Yan, *Adv. Mater*., **15**, 353 (2003).
3. J. Goldberger, A. I. Hochbaum, R. Fan and P. Yang, *Nano Lett*., **6**(5), 973 (2006).
4. B. Tian, X. Zheng, T. J. Kempa, Y. Fang, N. Yu, G. Yu, J. Huang and C. M. Lieber, *Nature*, **449**, 885 (2007).
5. K. Q. Peng, X. Wang, X. L. Wu and S. T. Lee, *Nano Lett*., **9**(11), 3704 (2009).
6. Y. Qu, L. Liao, Y. Li, H. Zhang, Y. Huang and X. Duan, *Nano Lett*., **9**(12), 4539 (2009).
7. V. Sivakov, G. Andra, A. Gawlik, A. Berger, J. Plentz, F. Falk and S. H. Christiansen, *Nano Lett*., **9**(4), 1549 (2009).
8. Y. Yao, M. T. McDowell, I. Ryu, H. Wu, N. Liu, L. Hu, W. D. Nix and Y. Cui, *Nano Lett*., **11**(7), 2949 (2011).
9. M. Ge, J. Rong, X. Fang and C. Zhou, *Nano Lett*., **12**(5), 2318 (2012).
10. K. Chen, B. R. Li and Y. Chen, *Nantod*., **6**(2), 131 (2011).
11. M. M. A. Hakim, M. Lombardini, K. Sun, F. Giustiniano, P. L. Roach, D. E. Davies, P. H. Howarth, M. R. R. Planque, H. Morgan and P. Ashburn, *Nano Lett*., **12**(4), 1868 (2012).
12. E. Ria, X. M. Liu, C. A. Ross, A. O. Adeyeye and W. K. Choi, *J. Appl. Phys.*, **112**(2), 024312 (2012).
13. J. Bauer, F. Fleischer, O. Breitenstein, L. Schubert, P. Werner, U. Gsele and M. Zacharias, *Appl. Phys. Lett*., **90**, 012105 (2007).
14. Y. H. Yang, S. J. Wu, S. H. Chiu, P. Lin and Y. T. Chen, *J. Phys. Chem. B*, **108**, 846 (2004).
15. K. K. Lew and J. M. Redwing, *J. Cryst. Growth*, **254**(1-2), 14 (2003).
16. H. Pan, S. Lim, C. Poh, H. Sun, X. Wu, Y. Feng and J. Lin, *Nanotechnology*, **16**, 417 (2005).
17. R. Q. Zhang, Y. Lifshitz and S. T. Lee, *Adv. Mater*., **15**(7-8), 635 (2003).
18. A. T. Heitsch, D. D. Fanfair, H. Y. Tuan and B. A. Korgel, *J. Am. Chem. Soc*., **130**(16), 5436 (2008).
19. K. J. Morton, G. Nieberg, S. F. Bai and S. Y. Chou, *Nanotechnology*, **19**, 345301 (2008).
20. H. D. Tong, S. Chen, W. G. van der Wiel, E. T. Carlen and A. van den Berg, *Nano Lett*., **9**(3), 1015 (2009).
21. S. T. Connor, M. X. Tang and Y. Cui, *Appl. Phys. Lett*., **93**(13),

133109 (2008).
22. K. Q. Peng, Y. J. Yan, S. P. Gao and J. Zhu, *Adv. Mater.*, **14**(16), 1164 (2002).
23. M. L. Zhang, K. Q. Peng, X. Fan, J. S. Jie, R. Q. Zhang, S. T. Lee and N. B. Wong, *J. Phys. Chem. C*, **112**(12), 4444 (2008).
24. H. Chen, H. Wang, X. H. Zhang, C. S. Lee and S. T. Lee, *Nano Lett.*, **10**(3), 864 (2010).
25. A. G. Nassiopoulou, V. Gianneta and C. Katsogridakis, *Nanoscale Res. Lett.*, **6**, 597 (2011).
26. K. Q. Peng, Y. Wu, H. Fang, X. Y. Zhong, Y. Xu and J. Zhu, *Angew. Chem. Int. Ed.*, **44**(18), 2737 (2005).
27. K. Q. Peng, J. J. Hu, Y. J. Yan, Y. Wu, H. Fang, Y. Xu, S. T. Lee and J. Zhu, *Adv. Funct. Mater.*, **16**(3), 387 (2006).
28. Z. P. Huang, H. Fang and J. Zhu, *Adv. Mater.*, **19**(5), 744 (2007).
29. K. Q. Peng, X. Wang, X. L. Wu and S. T. Lee, *Appl. Phys. Lett.*, **95**(14), 143119 (2009).
30. C. F. Pan, Z. X. Luo, C. Xu, J. Luo, R. R. Liang, G. Zhu, W. Z. Wu, W. X. Guo, X. X. Yan, J. Xu, Z. L. Wang and J. Zhu, *ACS Nano.*, **5**(8), 6629 (2011).
31. K. Q. Peng, Y. J. Yan, S. P. Gao and J. Zhu, *Adv. Funct. Mater.*, **13**(2), 127 (2003).
32. K. Q. Peng and J. Zhu, *J. Electroanal. Chem.*, **558**, 35 (2003).
33. K. Q. Peng, Y. Wu, H. Fang, X. Y. Zhong, Y. Xu and J. Zhu, *Angew. Chem.*, **117**(18), 2797 (2005).
34. A. B. D. Cassie and S. Baxter, *Trans. Faraday Soc.*, **40**, 546 (1944).
35. X. J. Huang, J. H. Lee, J. W. Lee, J. B. Yoon and Y. K. Choi, *Small*, **4**(2), 211 (2008).
36. F. Shi, Y. Y. Song, J. Niu, X. H. Xia, Z. Q. Wang and X. Zhang, *Chem. Mater.*, **18**(5), 1365 (2006).
37. B. B. Li, D. P. Yu and S. L. Zhang, *Phys. Rev. B*, **59**(3), 1645 (1999).
38. C. Li, G. Fang, S. Sheng, Z. Chen, J. Wang, S. Ma and X. Zhao, *Physica E*, **30**(1-2), 169 (2005).
39. K. W. Adu, H. R. Gutierrez, U. J. Kim and P. C. Eklund, *Phys. Rev. B*, **73**(15), 15533 (2006).
40. R. Gupta, Q. Xiong, C. K. Adu, U. J. Kim and P. C. Eklund, *Nano Lett.*, **3**(5), 627 (2003).